JOURNAL OF MATERIALS SCIENCE 32 (1997) 2963–2968

Wear mechanisms of Ti(C, N) ceramic in sliding contact with stainless steel

ZHAO XINGZHONG, LIU JIAJUN, ZHU BAOLIANG, MIAO HEZHUO, LUO ZHENBI
Tribology Research Institute, Tsinghua University, Beijing 100084, People's Republic of China

Austenic stainless steel AISI 321 is one of the most difficult materials to cut. In order to investigate the wear behaviour of Ti(C, N) ceramic when cutting the stainless steel, wear tests were carried out on a pin-on-disc tribometer, which could simulate a real cutting process. The selected load range is 58.8–235.2 N; the selected speed range is 0.8–3.2 m s^{-1}. The test results show that the wear of Ti(C, N) ceramic is mainly caused by adhesion between the rubbing surfaces; the wear increases with increasing load and increasing speed. When oil is used for lubrication, the friction coefficient of the sliding pairs and the wear rate of the ceramic are reduced. Scanning electron microscopy, energy-dispersive X-ray analysis and X-ray diffraction analysis are used to examine the worn surfaces. The wear mechanisms of Ti(C, N) ceramic sliding against the stainless steel are discussed in detail.

1. Introduction

Because of their excellent thermal and mechanical properties, ceramics have attracted much attention as structural materials. One of the most important uses of ceramics is for cutting tools, which are applied nowadays in turning cast iron and nickel-based alloys at high speeds [1, 2]. However, ceramic cutting tools are not universal for machining all metallic materials; for example, some reports show that Si_3N_4-based ceramics are suitable for machining cast iron, but unsuitable for machining steel, and one of the factors influencing this difference in behaviour is thought to be chemical dissolution of the ceramics in the chip at the high temperatures reached at the cutting edge [3]. The wear rate of a silicon nitride cutting tool is two orders of magnitude higher when machining AISI 1045 steel than when machining grey cast iron [4, 5]. Ti(C, N)-based ceramics are also important cutting tool materials; however, little knowledge about the wear behaviour of Ti(C, N)-based ceramics is available when they are used for cutting austenic stainless steels.

The objective of this study is to investigate the wear behaviours of a Ti(C, N)-based ceramic on a pin-on-disc tribometer under dry and lubricated conditions. In comparison with real machine tests, pin-on-disc tests are simple and quick and the conditions in which they can be employed may be widely varied and well controlled; they seem to be appropriate tests for tool life simulation. Some work has been done on the wear mechanism analysis of ceramic tool materials and the comparison of wear data from pin-on-disc tests and cutting behaviours of ceramics [6, 7]. In this study, the worn surfaces of the Ti(C, N) ceramics were examined and analysed using scanning electron microscopy (SEM), electron probe microanalysis (EPMA) and energy-dispersive X-ray analysis (EDXA).

2. Experimental procedure

2.1. Test machine and specimens

Wear tests are carried out on a pin-on-disc tribometer. The pin specimen is fixed; the disk specimen, driven by a motor, can rotate at different speeds. A schematic diagram of the tester is shown in Fig. 1. The initial line contact model was formed between the pin and the disc, which can simulate the contact form of cutting tool and workpiece in real cutting practice. The angle of inclination of the pin is 80°; so the wear volume can be calculated from the following formula:

$$\text{wear volume} = 0.5LB^2 \sin 10^\circ \cos 10^\circ$$

In this formula, L is the length of the ceramic wear scar (5 mm in this test) and B (mm) is the width of the wear scar. The above formula can be simplified to $V_W = 0.427B^2$ (mm^3).

The pin is made from hot-pressed Ti(C, N) ceramic, having a size of 5 mm × 5 mm × 25 mm; the disc was machined from AISI 321 stainless steel, 56 mm in diameter and 6 mm in thickness. The roughnesses, as measured by stylus profilometry, of the pin and the disc are $R_a = 0.32$ μm and $R_a = 0.21$ μm, respectively. Some properties of the Ti(C, N) ceramic are listed in Table I.

2.2. Test method

Friction and wear tests are operated under dry and lubricated conditions. The room temperature is about 20 °C. Liquid paraffin containing 2 wt% of zinc

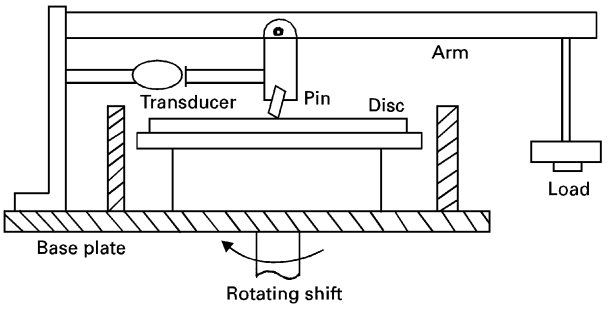

Figure 1 The schematic diagram of the tester.

TABLE I Physical and mechanical properties of the Ti(C, N) ceramic

Property	Units	Value
Amount	wt %	Ti(C, N) > 80
Grain size	μm	< 1
Density	g cm^{-3}	4.88
Vicker's hardness	HV	1850
Bending strength	MPa	750
Fracture toughness	MPa m$^{1/2}$	4.7
Impurities		Al_2O_3, ZrO_2

dialkyl dithiophosphate (ZDDP) additive is used for lubrication; its kinematic viscosity at 25 °C is 30 mm^2 s^{-1}. During the operating process, the lubricating oils are fed into the contact point between the pin and the disc by natural falling flow from a reservoir. The average rate of the flow is about 0.01 l min^{-1}. The sliding speeds between the rubbing surfaces are 0.8–3.2 m s^{-1}; the selected load range is from 58.8 to 235.2 N. Each pair of the samples has a 30 min running time under a selected speed and load. At least two tests were performed, controlling the standard deviation of the results to less than ± 6%. Before and after testing, the specimens were ultrasonically cleaned in an acetone bath for 15 min and then in a hexane bath for 2 min.

The wear scar width of the pin is measured under a photo microscope; then the volume and wear rate can be calculated. (When severe metal transfer occurs, the transfer layer is firstly etched away; then the wear scar width of the ceramic pin is measured.) The frictional force is transmitted by a transducer to a recorder continuously during the test, from which the friction coefficient can be obtained. The worn surfaces are examined by using SEM, EDXA and X-ray diffraction (XRD).

3. Results and discussion

3.1. Effects of load on friction coefficient and wear rate

Figs 2 and 3 show the variations in friction coefficient and wear rate with load, respectively. It can be seen from the figures that the friction coefficient and wear rate of the ceramic increase with increasing load in dry conditions. In oil-lubricated conditions, the friction coefficient and the wear rate obviously decrease but

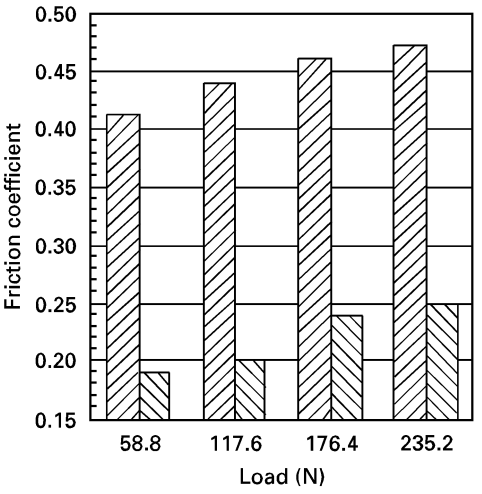

Figure 2 Variation in friction coefficient with load. (▨), dry; (▧) oil lubricated.

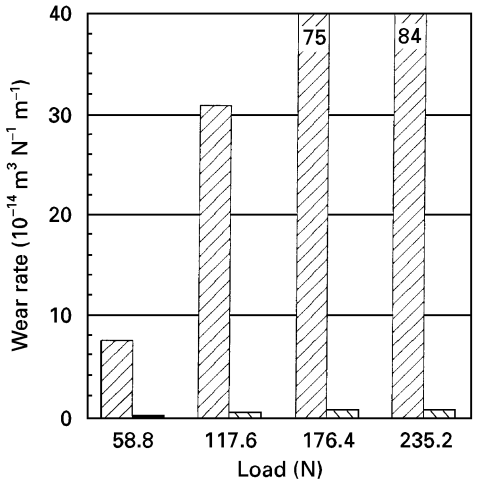

Figure 3 Variation in wear rate of the ceramic with load. (▨), dry; (▧), oil lubricated.

both still increase with increasing load. In dry conditions, stainless steel transfers on the worn ceramic surfaces at both low and high loads (Fig. 4). The rapid increase in the wear rate under dry conditions in the higher load range (176.4–235.2 N) may be caused by severe adhesion between the rubbing surfaces and the increase in the microfracture of the ceramic; the latter is confirmed by the SEM examinations of the worn Ti(C, N) ceramic surface and the wear debris (Figs 5 and 6). The arrow in Fig. 5 points to the microfracture pit. Fig. 6a shows a microfracture fragment of the ceramic; its EDXA spectrum is shown in Fig. 6b, which further indicates that the particle comes from the Ti(C, N) ceramic. The use of the lubricating oils reduced the friction traction on the rubbing surfaces [8] and hence the stresses transmitted to the ceramic from the stainless steel; this also reduced operating stresses below the limit for fracture of the ceramic. Furthermore, as the friction coefficient is reduced, the maximum shear stress will move from the surface into the bulk of the material. Since most microfracture is surface dominated, this will have the effect of reducing fracture of the ceramic. So the wear rate of Ti(C, N)

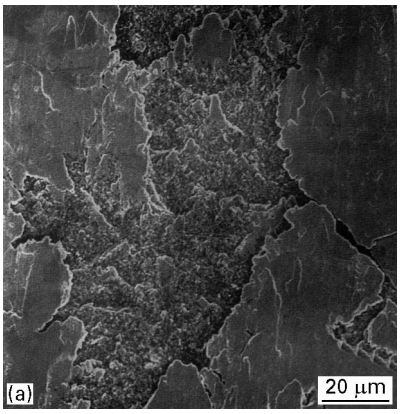

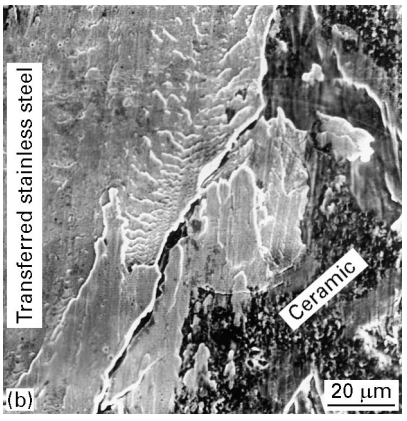

Figure 4 SEM morphologies of the worn ceramic surfaces; (a) dry, 117.6 N, 1.6 m s^{-1}; (b) dry, 235.2 N, 1.6 m s^{-1}.

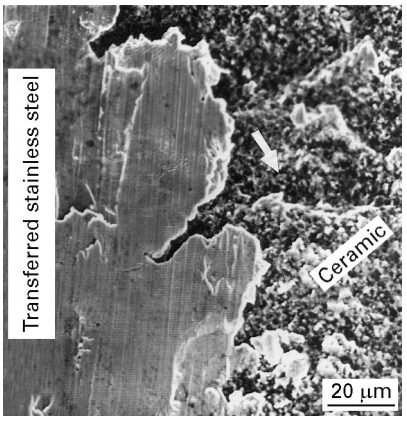

Figure 5 SEM morphology of the worn ceramic surface (dry; 235.2 N; 1.6 m s^{-1}).

ceramic is reduced much more in the higher load range compared with dry friction conditions.

3.2. Effects of speed on friction coefficient and wear rate

The variations in friction coefficient and wear rate with speed are shown in Figs 7 and 8. Under dry conditions, the friction coefficient increases with increasing speed in the lower speed range (0.8–1.6 m s^{-1}) and reaches its maximum at 1.6 m s^{-1} and then decreases slightly with increasing speed. The wear rate of the ceramic has a minimum value at the speed of 2.4 m s^{-1}. The lower friction coefficient and higher

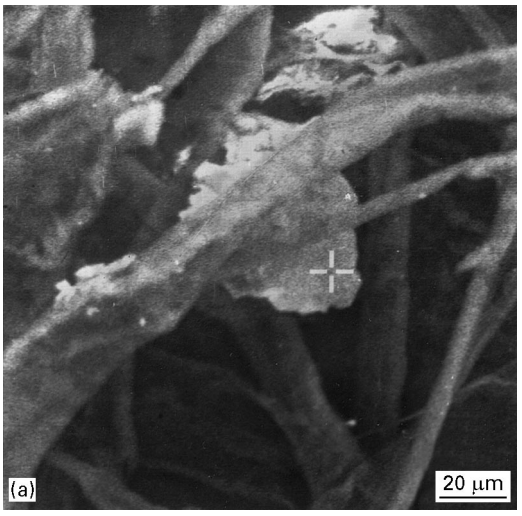

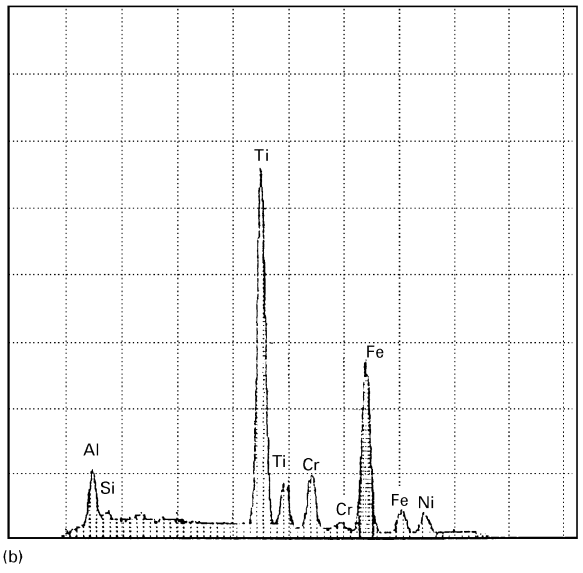

Figure 6 SEM examinations of the wear debris; (a) microfracture fragments; (b) EDXA spectrum of the point indicated in (a).

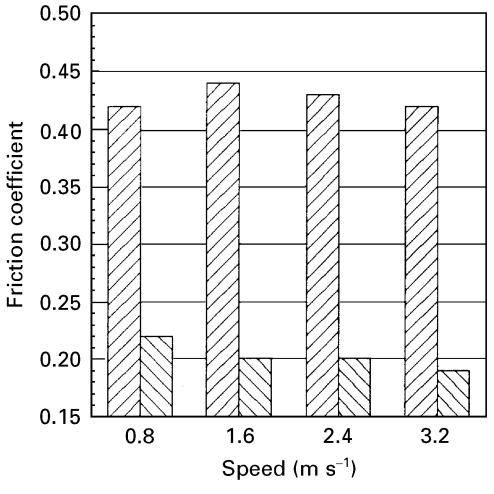

Figure 7 Variation in friction coefficient with speed. (▨), dry; (▧), oil lubricated.

wear rate at the high speed (3.2 m s^{-1}) may be attributed to the melting of some ceramic grains on the rubbing surfaces, which is confirmed by the SEM and EDXA examinations (Figs 9 and 10). The morphology

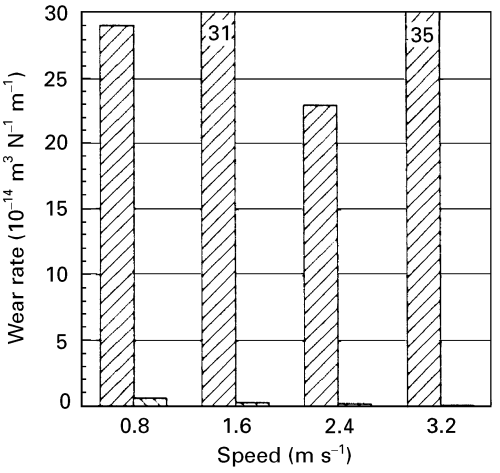

Figure 8 Variation in wear rate of the ceramic with speed, (▨), dry; (▧), oil lubricated.

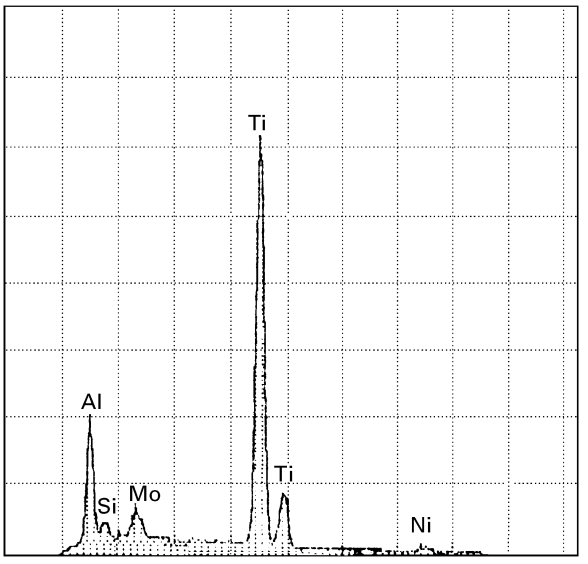

Figure 10 EDXA spectrum of the point indicated in Fig. 9c.

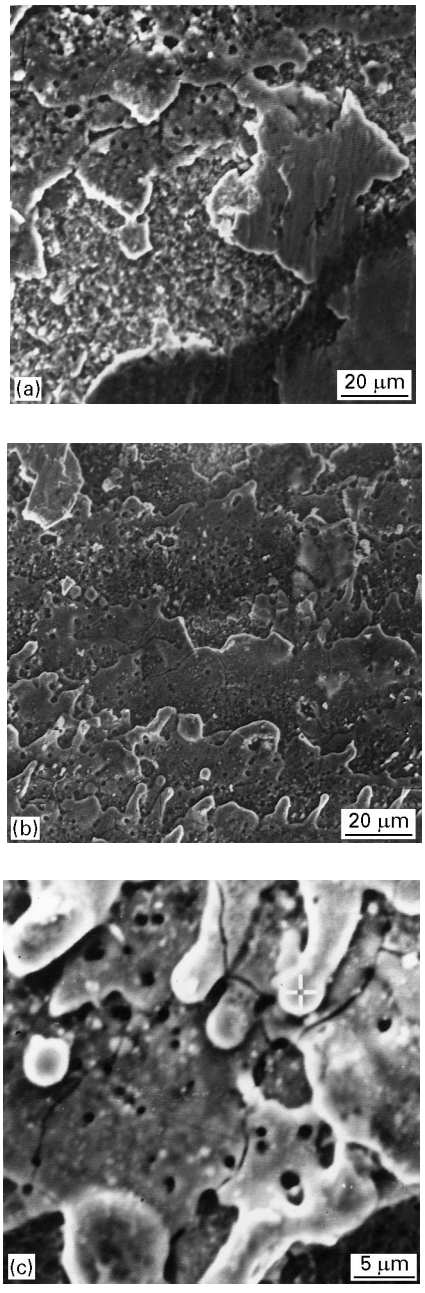

Figure 9 SEM morphologies of the worn ceramic surfaces; (a) dry, 117.6 N, 2.4 m s^{-1}; (b), (c) dry, 117.6 N, 3.2 m s^{-1}.

in Fig. 9 suggests the presence of a liquid phase during the rubbing operation. The EDXA spectrum of the marked point in Fig. 9c is shown in Fig. 10, which indicates that the molten material comes only from the ceramic because no Fe element appears in the spectrum. It seems hard to understand the ceramic melting, but the following facts can explain the possibility to some extent. First, the ceramic is composed of not only TiN or TiC, but also many additives, such as Al_2O_3, ZrO_2, MgO, Ni and Mo, which may combine with TiC or TiN to form low-melting point eutectics and reduce the melting point of the ceramic. In [9], when a ceramic cutting tool containing ZrO_2, TiC and TiN inclusions was used to cut AISI 1040 steel, it was also found that a liquid phase formed on the flank of the ceramic tool during cutting process, which is consistent with the presence of two eutectics at 1085 and 1289 °C, respectively, in the Fe–Ti phase diagram [10]. Second, the heat conductivity of the ceramic is rather poor. Third, a large amount of deformation heat and friction heat will be produced in the rubbing process because of the very high toughness of the stainless steel and the relatively low heat conductivity (compared with carbon steel). Fourth, the small contact area of the ceramic sample maintains the contact state during the whole rubbing process; the temperature of its contact surface could be much higher than that of the stainless steel surface. All these factors result in very high temperatures on the rubbing surfaces, especially on the rubbing ceramic surface, which cause the ceramic grains to melt.

Compared with dry conditions, the friction coefficient and wear rate are reduced because of the lubricating and cooling effects of the lubricating oil, especially because of the tribochemical effects of the additive ZDDP. This result is consistent with the result of [11]. Under lubricated conditions, no molten materials were found on the worn ceramic surfaces; in addition, the amount of the transferred stainless steel is reduced compared with dry conditions (Fig. 11). In order to determine the tribochemical mechanism of

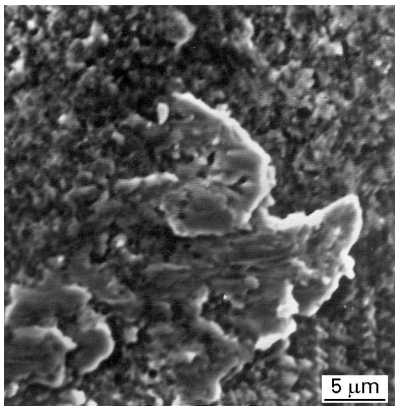

Figure 11 SEM morphology of the worn ceramic surface (oil lubricated; 117.6 N; 2.4 m s^{-1}).

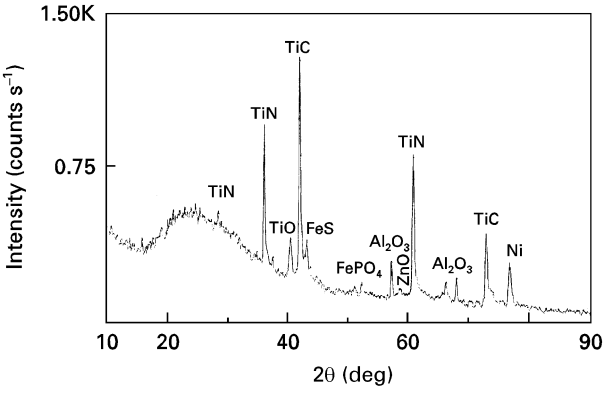

Figure 12 XRD spectrum of the worn ceramic surfaces (oil lubricated; 117.6 N; 2.4 m s^{-1}).

the antiwear additive ZDDP, XRD was used to examine the worn surfaces of the ceramic; the result is shown in Fig. 12. The XRD spectrum indicates that tribochemical reaction products are formed on the worn ceramic surface, from which the tribochemical reaction mechanisms may be described as follows. Firstly, ZDDP decomposes thermally by β-hydrogen elimination and nucleophilic substitution, forming a series of products, e.g., olefin, H_2S, RSR, RSH, RSSR, $(SR)_3PS$, ZnO, zinc pyrothiophosphates and polypyrothiophosphates [12]. The decomposed products then react with the transferred stainless steel, forming FeS, $FePO_4$, FeO, etc. TiO_2 may be the oxidation product of TiC and/or TiN. The tribochemical reaction processes can be represented as the following formulae:

$$\text{ZDDP} \rightarrow H_2S, \text{RSH, RSSR, ZnO, etc.}$$
$$H_2S, \text{RSH or RSSR} + \text{Fe} \rightarrow \text{FeS}$$
$$\text{Fe} + \text{polypyrothiophosphates} \rightarrow FePO_4$$
$$\text{TiC or TiN} + O_2 \rightarrow TiO_2$$

where R is an alkyl group.

The tribochemical products are very effective in reducing adhesive wear and microfracture wear of the ceramic.

3.3. Wear mechanisms of Ti(C, N) ceramic

In order to reveal the wear mechanism of Ti(C, N) ceramic, SEM was used for examination of the worn surfaces. The SEM morphologies of the worn ceramic surfaces at different loads are shown in Fig. 4. It can be seen from the figures that stainless steel transfers on the ceramic surfaces because of adhesion between the rubbing surfaces. It can also be found by comparing Fig. 4a and b that the amount of the transferred stainless steel increases with increasing load, and many larger transferred stainless steel flats formed on the worn ceramic surface at the higher load (235.2 N), while only smaller stainless steel flats formed at the lower load (117.6 N); this shows that the adhesion between the rubbing surfaces became more severe with increasing load; so both the friction coefficient and the wear rate increased. This result could be attributed to the effects of the native oxide on the stainless steel. At low loads, the ceramic will slide against the native oxide; the friction and adhesion will be low. At a certain load the native oxide will crack, exposing unoxidized steel during sliding which is highly reactive and will adhere to the Ti(C, N) ceramic. This will be a localized effect but, as the load increases, the number of regions of oxide breakdown and hence the amount of adhesion and transfer will increase.

From the test results and the examinations, it is not difficult to deduce the wear mechanisms of the ceramic. In dry conditions (at a sliding speed less than 1.6 m s^{-1}), the wear of the ceramic is mainly caused by the adhesion between the rubbing surfaces. Strong adhesion occurs when the ceramic and stainless steel are put into sliding contact (especially at higher loads). With the relative movement of the rubbing surfaces, the adhesive junctions or areas are torn off, resulting in the transfer of stainless steel on the rubbing ceramic surface. (The adhesive junctions or areas may be broken more frequently in stainless steel surface because of its relatively low shearing strength.)

The transferred stainless steel on the ceramic surface is subjected to shear and compressive stresses repeatedly with the rubbing movement, which may cause microcracks and microfractures in the ceramic surface or its subsurface. Meanwhile, the transferred stainless steel is also subjected to an adhesive force from the rubbing stainless steel surface, which will peel off the transferred stainless steel flats. Ceramic microfracture pieces or ceramic grains will also be peeled off or pull out and leave the ceramic surface with the peeled-off stainless steel flats, which gives rise to the wear of the ceramic. With increasing load, adhesive wear gradually occurs. In addition, microfracture wear of the ceramic becomes very severe when the load is increased over a certain value (176.4 N in this test). Microfracture brings about a much higher wear rate of the ceramic than does adhesion. In addition, it is also possible that the microfracture ceramic particles embedded in the transfer layer cause three-body abrasion to the ceramic, leading to increased ceramic wear rates [13].

The lubricating oil, especially containing the antiwear additive ZDDP, prevents adhesion between the rubbing surfaces; moreover, it reduces operating stresses below the limit for fracture of the ceramic; so the friction coefficient and wear rate are reduced in lubricated conditions.

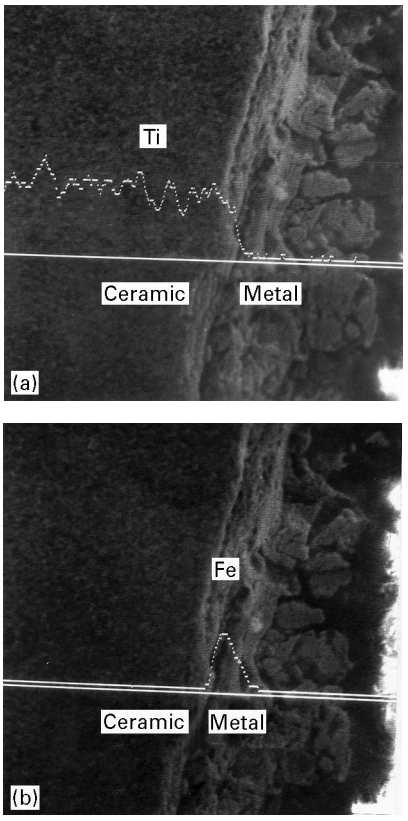

Figure 13 Element diffusion between ceramic and stainless steel; (a) Ti diffusion in stainless steel; (b) Fe diffusion in ceramic.

3.4. Melting of Ti(C, N) ceramic grains and element diffusion

In addition to the adhesion–peeling-off and microfracture wear mechanisms mentioned above, wear of the ceramic is also attributed to the melting of the ceramic grains and the element interdiffusion between the rubbing surfaces. At the high sliding speed (3.2 m s^{-1} in this test), the ceramic grains melt (see Figs 9 and 10). The molten regions were scattered on the worn ceramic surface. So, in this condition, the wear of the ceramic is also caused by melting of the ceramic in addition to adhesion. In the rubbing process, the molten ceramic is extruded away, resulting in wear of the ceramic.

In order to clarify the element interdiffusion between the rubbing surfaces, the transverse section of the worn ceramic surface was examined using SEM and EDXA. Fig. 13 shows that element interdiffusion occurs between the worn ceramic surface and the transferred stainless steel flats. The interdiffusion of Ti and Fe elements will make the adhesion between the rubbing surfaces more severe. In addition, the diffusion of Ti element in stainless steel will also result in destruction of the structure and a decrease in the strength of the ceramic surface, which will accelerate wear of the ceramic. The lubricating oil and the additive decrease the adhesion, the temperature of the rubbing surfaces and the element interdiffusion; so the friction coefficient and wear rate are reduced.

4. Conclusions

From the above test results and surface examinations, the following conclusions can be summarized.

1. In Ti(C, N) ceramic–stainless steel sliding contacts, the wear of the ceramic is mainly caused by the adhesion–peeling-off process. Stainless steel firstly transfers on the ceramic surface; then the transferred stainless steel flats are subjected to repeated shearing and compressive stresses until they are peeled off the rubbing ceramic surface. When the transferred stainless steel flats are peeled off the ceramic surface, some ceramic fragments or its grains also pull out and are moved away. A higher load causes more severe adhesive wear and microfracture wear of the ceramic.

2. At high sliding speeds, more friction heat and element interdiffusion (compared with low sliding speeds) make the adhesive wear of the rubbing ceramic surfaces more severe. In addition, the melting of the ceramic grains also causes severe wear of the ceramic.

3. With increasing load and increasing speed, the friction heat of the rubbing surfaces increases rapidly, which will accelerate the melting of the ceramic grains and adhesion between the rubbing surfaces; so the wear of the ceramic increases with increasing load and increasing speed.

4. Because of its lubricating and cooling actions, the oil reduced the friction coefficient and wear rate of the Ti(C, N) ceramic–stainless steel sliding pairs, which suggests that appropriate lubrication and cooling are useful and helpful for reduction in wear of ceramic cutting tools in real cutting processes, and certainly, more research work on this should be done in the future.

Acknowledgements

The authors would like to thank the National Natural Sciences Foundation of China and the Laboratory of Solid Lubrication, Lanzhou Institute of Chemical Physics, Chinese Academy of Sciences, for their financial support for this project.

References

1. T. N. BLACKMAN, *Foundryman*, **3** (1990) 17.
2. J. AUCOTE and S. R. FOSTER, *Mater. Sci. Technol.* **2** (1986) 700.
3. J. VLEUGELS, T. LAOUI, K. VERCAMMEN, J. P. CELIS and O. VAN DER BEST, *Mater. Sci. Engng* **A187** (1994) 177.
4. E. K. ASIBU, *J. Manuf. Syst.* **9** (1990) 159.
5. M. K. BRUN and M. LEE, *Ceram. Engng. Sci. Proc.* **4** (1983) 646.
6. R. RIGAUT, Y. M. CHEN and J. SAINT CHELY, *Lubr. Engng.* **50** (1994) 485.
7. G. BRANT, A. GERENDAS and M. MIKUS *J. Eur. Ceram. Soc.* **6** (1990) 273.
8. D. H. BUCKLEY and K. MIYOSHI, *Wear* **100** (1984) 333.
9. S. L. CASTO, E. L. VALVO, V. F. RUISI, E. LUCCHINI and S. MASCHIO, *ibid.* **160** (1993) 227.
10. Th. MASSALSKI, J. J. H. BENNET and H. BAKER (eds), "Binary alloy phase diagrams", Vol. 2 (American Society for Metals, Metals Park, OH, 1987).
11. H. K. TONSHOFF, H. G. WOBKER and D. BRANDT, *Lubr. Engng.* **50** (1995) 163.
12. WEI JIANJUN and XUE QUNJI, *Wear* **162–4** (1993) 1068.
13. P. Q. CAMPBELL, J. P. CELIS, J. R. ROOS and O. VAN DER BIEST, *Wear* **174** (1994) 47.

Received 19 April
and accepted 14 December 1996